ACS OMEGA

http://pubs.acs.org/journal/acsodf
Article

Introducing Water Electrolithography

Sumit Kumar, Ebinesh Abraham, Praveen Kumar,* and Rudra Pratap

Cite This: *ACS Omega* 2021, 6, 25692−25701 Read Online

ACCESS | Metrics & More | Article Recommendations | Supporting Information

ABSTRACT: High-resolution patterning with remarkable customizability has stimulated the invention of numerous scanning probe lithography (SPL) techniques. However, frequent tip damage, substrate-film deterioration, low throughput, and debris amassing in the patterned region are the inherent impediments that have precluded obtaining patterns with high repeatability using SPL. Hence, SPL still has not got wider acceptance for industrial fabrication and technological applications. Here, we introduce a novel SPL technique, named water electrolithography (W-ELG), for patterning at the microscale and potentially at the nanoscale also. The technique operates in the non-contact mode and is based on the selective etching, via an electrochemical process, of a metallic film (e.g., Cr) submerged into water. Here, the working of W-ELG is demonstrated by scribing a pattern into the Cr film by a traversing cathode tip along a preset locus. A numerical analysis establishing the working principles and optimization strategies of W-ELG is also presented. The tip-sample distance and tip-diameter are identified as the critical parameters controlling the pattern creation. W-ELG achieved a throughput of 1.5×10^7 μm^2/h, which is the highest among the existing SPL techniques, while drawing 4 μm wide lines, and is also immune to deleterious issues of tip damage, debris amassment, etc. Therefore, the resolution of these inherent impediments of SPL in W-ELG sets the stage for a paradigm shift that may now translate the SPL from academic exploration to industrial fabrications.

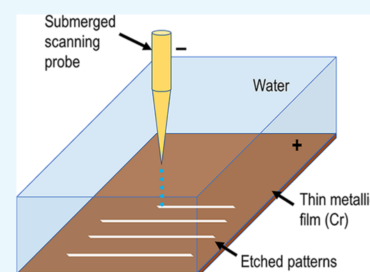

1. INTRODUCTION

The fabrication of microelectronic devices and micro-/nano-electro-mechanical systems (MEMS/ NEMS) devices depends on the accuracy and precision of pattern creation at a very small length scale, ranging from micrometers to nanometers. Therefore, patterning and lithography are vital steps in the fabrication of these small length-scale devices. The never-satiating trend of miniaturization and mass production of micro-and nanosystems require device fabrication using lithography techniques that can create high-resolution patterns at high throughput and with reasonable flexibility to allow batch-customization[$]. Traditionally, photolithography (PL) and e-beam lithography (EBL) have been the lithography techniques of choice for micro-and nanofabrication in both academia and industries.[1−7] Although the throughput of photolithography, which is a mask-based "flood-exposure" type technique, is the highest among all lithography techniques, its resolution is limited by the wavelength of the light used for the photoresist exposure. Therefore, the resolution of photolithography is often in the micrometer or higher submicrometer regime.[8] On the other hand, the pattern resolution of EBL is limited by the diameter of the electron beam and the secondary-electron interaction volume, which can be as small as a few nanometers; however, the throughput for EBL, which is a scanning-based technique, is very low.[8−11] Therefore, currently, there is a pressing need of a versatile "high resolution-high throughput" lithography technique, as either the lithography processes can produce patterns with high resolution at low throughput or at high throughput with relatively poorer resolution. This apparent paradox is often represented in terms of Tennant's law.[12] Hence, the development of a new versatile lithography tool, resolving the resolution-throughput paradox, remains a highly active area of research, garnering significant interest among both scientists and technologists in the recent past.

In the past few decades, photolithography has witnessed major upgradation, such as the development of deep-ultraviolet (DUV) and extreme-ultraviolet (EUV) lithography techniques,[2,13−17] which has led to significant improvement in the throughput-resolution combination. DUV and EUV have been adopted for the fabrication of the new generation of microelectronic chips. However, both the resolution and the customizability of scanning-based techniques, such as EBL, have been unattainable in photolithography, including EUV and DUV. Inspired by the goal of increasing the throughput while maintaining the flexibility (or batch customizability) and the resolution generally associated with a scanning-based method, a plethora of scanning probe lithography (SPL) techniques have emerged as alternative lithography processes. The basic working principle of all SPL techniques is the modification of the surface of a substrate using a sharp probe

Received: July 20, 2021
Accepted: September 10, 2021
Published: September 21, 2021

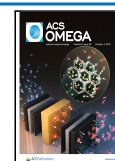

ACS Publications
© 2021 The Authors. Published by American Chemical Society

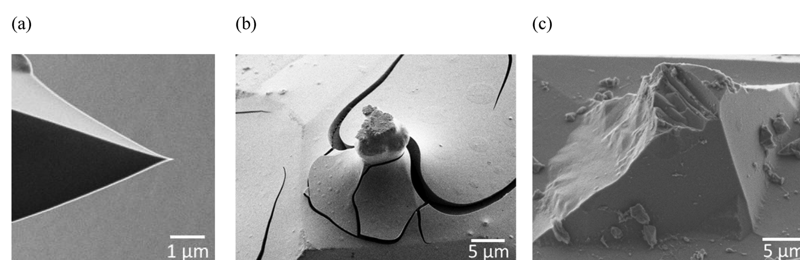

Figure 1. SEM micrographs showing an AFM-tip used for patterning using ELG, one of the promising SPL techniques for its ability to create high-resolution patterns in both direct and indirect modes: (a) before and (b, c) after pattern "writing". The cracked surface and the accumulation of material at the tip in (b) is the reaction product, CrO_3, formed due to the chemical reaction between Cr and water vapor. Micrograph in (c) shows an example case where an AFM tip is broken due to the bending force applied on it by the friction present during the contact-mode operation of ELG. As the chemical reaction product sticks to the tip or the tip is broken, either the electric circuit between the two electrodes is broken or the effective tip radius increases, leading to an unexpected change in the profile of the trench created in Cr. Besides limiting the life of the tip, these issues also lead to the non-repeatability of patterns created.

tip.[6,18] Therefore, various SPL techniques have evolved depending on the nature of the interaction between the tip and the surface, such as oxidation-SPL, thermal-SPL, field-emission SPL,[19] mechanical-SPL, dip-pen nanolithography (DPN), electrolithography (ELG),[£] etc.[6,20] The flexibility in manipulating the tip-substrate surface interaction proffers SPL to be suitable for both direct writing (such as DPN, ELG in oxidation mode,[21,22] etc.) and indirect patterning (such as ELG in the trench-creation mode,[23,24] etc.) that can be used to transfer the pattern to the material of choice, e.g., metal, semiconductor, ceramic, polymer, protein, etc.[6,10−12] In addition, SPL techniques, which are often inexpensive to establish and maintain as compared to EBL[€], EUV, etc., allow parallelization of processing: Herein, numerous tips can be independently controlled to write complex patterns in high throughput fashion as well as with enormous flexibility (or batch customizability).[25,26] Due to these advantages, SPL has become one of the most researched lithography techniques in the last few decades.[6]

Traditionally, SPL has relied upon standard tip-containing equipment with extremely sophisticated systems for controlled movement of the tip, such as atomic force microscope (AFM) and scanning tunneling microscope (STM), for patterning. As a direct-writing SPL process, STM has been used for localized anodic oxidation of various metals, such as chromium (Cr), molybdenum (Mo), etc., in "proximity" mode to create patterns with a high resolution of 25 nm and better.[21,22] The formation of nanostructures, with feature sizes as small as 20 nm, by means of electric field-induced oxidation of metal films using AFM tips has also been reported.[27−29] Using the AFM platform, ELG has been shown to create linear patterns having a width of as low as 8 nm in a polymer and 40 nm in the transferred metal.[23,24] These examples clearly demonstrate the ability to write patterns with resolution quite close to that of EBL using electric-field-based SPL techniques. Since every single locus of the tip in AFM and STM can be customized, SPL, including ELG, facilitates remarkable flexibility in writing patterns. Furthermore, in the case of ELG, the same setup has been used to create patterns with width varying over four orders of magnitude by varying the electric potential applied between the tip and the substrate and the velocity of the tip.[24] However, using setups primarily designed for surface topography mapping, i.e., AFM and STM, for SPL greatly limits the scope for parallelization and adds to the cost of the lithography setup. Furthermore, these tools are not meant to work beyond a certain proximity to the sample and hence they cannot be used to develop any meaningful non-contact SPL technique. Hence, there is a need to develop a dedicated stylus-based setup for SPL.

Although SPL, especially ELG, exhibits advantages of high resolution, flexibility (or batch-customizability), creating patterns in both direct and indirect fashion, and potentially high throughput (e.g., via parallelization of tips, increasing tip velocity, increasing tip-to-sample potential, etc.), there are a few innate obstructions that hamper the acceptance of the SPL as a substitute for EBL and photolithography for commercial purposes. Some of these are tip and sample damage due to the high friction,[23,30] accumulation of the reaction product in and near the patterned trench as well as the tip (see Figure 1) that affects the quality and repeatability of the patterns,[30] low throughput as the tip velocity cannot be increased arbitrarily fast without compromising the time required for completing tip-sample interaction, etc. Figure 1a shows an AFM probe before pattern drawing in a Cr film in contact mode using ELG. A straight-line pattern is drawn in 40 nm-thick Cr film deposited on a SiO_2/Si substrate by applying a tip bias of −4 V and at a speed of 10 μm/s. The chemical product (CrO_3) formed during the patterning sticks to the tip and prohibits further patterning (see Figure 1b). Figure 1c shows an AFM probe damaged during the scratch lithography patterning in the Cr thin film on PMMA coated on the Si/SiO_2 substrate. An unbalanced tip force and repeated patterning lead to such a problem. In addition, the maximum throughput of only $\sim 10^5$ μm^2/h has been reported for various SPLs in comparison to $\sim 10^{10}$ μm^2/h for photolithography.[6] Realizing that the fundamental origin of the above sets of inherent deleterious issues related to the SPL lies in the fact that the scribing tip and the substrate remain in contact (or in close proximity) throughout patterning, an obvious way to alleviate these issues is by developing an SPL method that works under non-contact mode. Here, we introduce a novel technique of pattern drawing called water-electrolithography (W-ELG), which works in non-contact mode and hence resolves all the above issues while retaining the advantages of SPL techniques, such as high resolution, high flexibility, potential parallelization, and the ability to create patterns in both direct and indirect modes. Furthermore, the electro-etching in W-ELG occurs at an unprecedently high rate, allowing patterning at a high throughput that may be the highest of all known SPL techniques. Herein, besides demonstrating the workings of the W-ELG at the microscale, we also discuss the roles of various critical parameters in controlling the patterns created

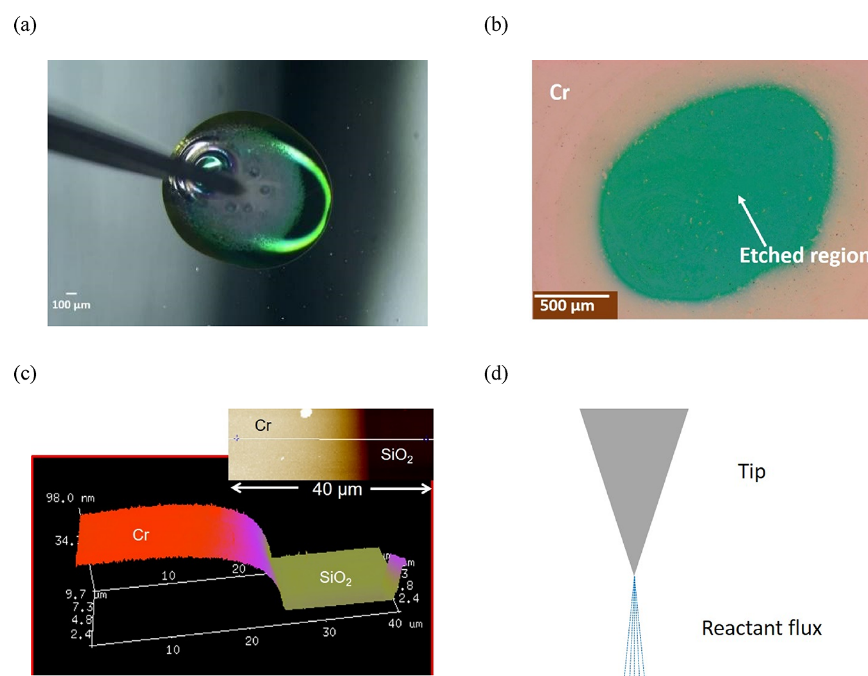

Figure 2. Electro-etching of the Cr film deposited on the SiO_2/Si substrate in the presence of water in between the cathode tip and the sample: (a) Digital picture showing a moment after a cathode tip is placed inside a water droplet without making contact with the Cr film and applying an electric potential between the tip and the sample. The picture shown here is a snapshot of the video shown in Video S1. (b) Optical micrograph of the region in the Cr film that is electro-etched in the presence of water droplet, and (c) surface topography, obtained using AFM, near one of the edges of the electro-etched region, showing rounding of the edge. The inset in panel (c) shows the sample near the edge of the electro-etched region. (d) Schematic illustrating the formation of a vortex due to movement/flux of the oxygen ions and reaction product (Video S2). For the samples shown here, the thickness of the Cr film was 100 nm, whereas the thicknesses of the thermally grown SiO_2 and Si substrate were 1 and 500 μm, respectively. A tip potential of 10 V was applied.

using W-ELG and, hence, provide cues that can potentially be used to pattern at the nanoscale.

2. DETAILS OF W-ELG

2.1. Working Principle of W-ELG. Figure 2 demonstrates the phenomenon of electro-etching of a metal film in the presence of a water layer between the metal film and the tip, which forms the basis of W-ELG (see Video S1 for a video of the process). Here, a small volume of deionized (DI) water is drop-cast, using a micropipette, on the Cr film, and the cathode tip is dipped into the water droplet without touching the Cr film (see Figure 2a, which shows the cathode tip). The anode probe tip is kept in contact with the Cr film, sufficiently far away from the cathode tip so that a limited movement of the cathode tip does not substantially change the radially symmetric profile of the electric field in the Cr film in the vicinity of the cathode tip. Subsequently, a potential difference (e.g., 10 V in the case shown in Figure 2) is applied between the two electrodes, and a vigorous chemical reaction, distinctively marked by effervescing gas bubbles emanating near the cathode, is observed (see Video S1). The color of the "water" droplet becomes yellowish due to the dissolution of the new chemical compound (CrO_3)[30] formed due to the chemical reaction between Cr and oxygen, which is present at the anode (i.e., near Cr film, which is one of the reactants) due to the electrolysis of the water. In practice, due to the high solubility of CrO_3 in water, the reaction product is completely removed from the region below the cathode tip; this is confirmed via a series of characterizations performed using an optical microscope, a scanning electron microscope (SEM), and an AFM (see Figure 2b,c). Figure 2c shows a topographic map, obtained using an AFM, of the edge of the electro-etched region. Figure 2c confirms almost vertical etching of the Cr film, except for the top edge that becomes rounded.

Now, noticing the potential of performing the chemical reaction inside a water droplet below the cathode tip, further experiments were also carried out while submerging the entire sample (or workpiece) and both the electrodes inside the DI water. Reaction profiles identical to that shown in Figure 2 were observed, and the Cr could be removed selectively from the film near the cathode tip, leaving a circular trench in its vicinity and exposing the SiO_2/Si substrate. Furthermore, when the cathode tip was traversed over the Cr film in the non-contact mode while keeping the sample and both electrodes submerged in DI water, the Cr immediately below the cathode tip continued to react with water to form CrO_3, as is evident from the formation of a vortex-like feature (Figure 2d). The vortex-like feature forms due to the amalgamation of the transport of oxygen ion formed at the cathode (where, as will be explained later, the electric field is highly concentrated) to the anode (in a rather streak fashion − see Video S2) and the transport of the hydrogen as well as oxygen (leftover from the reaction) gases to the surface of the water. When the sample is removed from the water following the electro-etching process, the Cr film is observed to be selectively removed from the region where the cathode tip has been traversed. This confirms the occurrence of a chemical reaction and removal of the chemical reaction product from the Cr film simultaneously even under the dynamic condition (i.e., when the stylus/tip is traversing in the non-contact mode). Based on these observations, we conceived the idea of W-ELG, a novel non-contact SPL technique, for patterning.

https://doi.org/10.1021/acsomega.1c03858
ACS Omega 2021, 6, 25692−25701

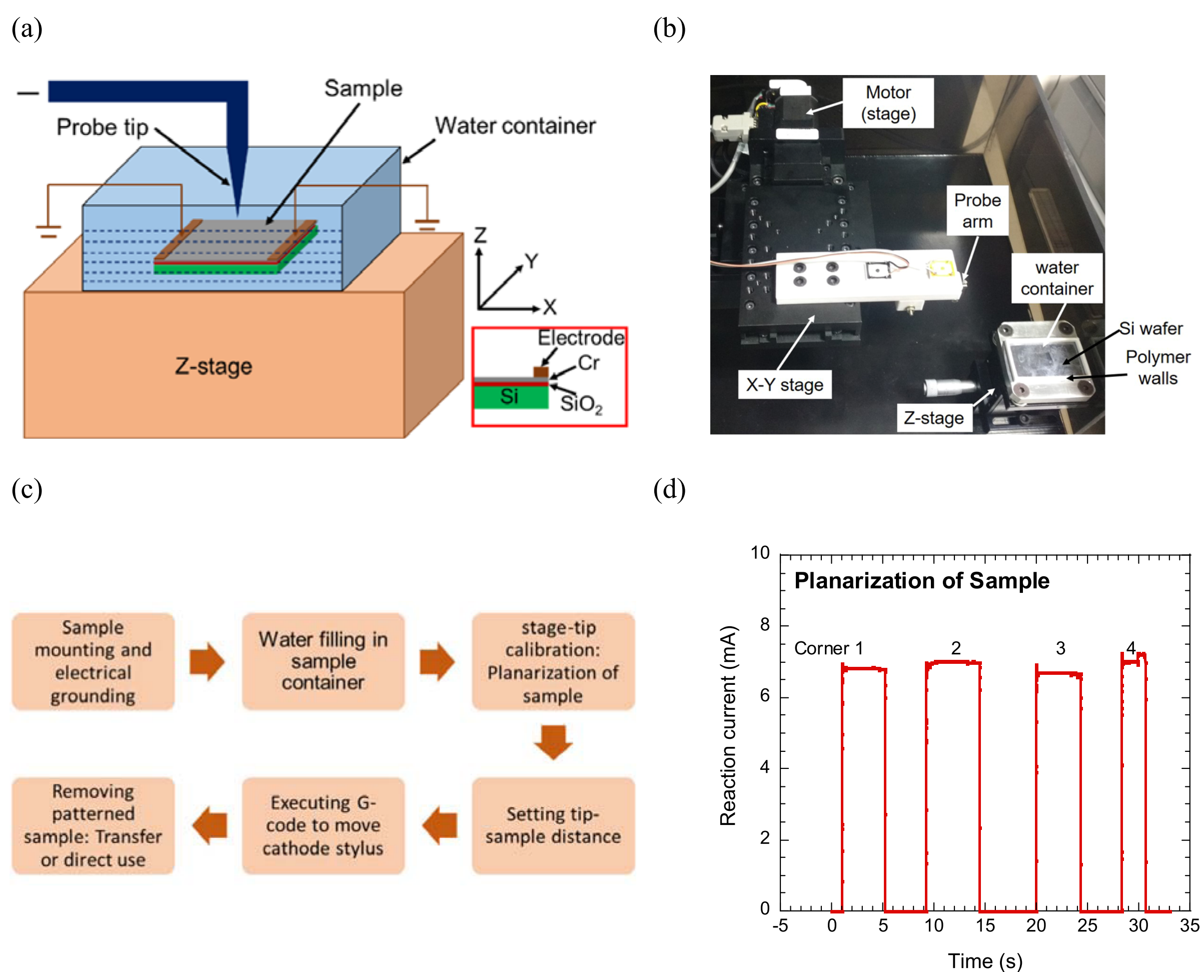

Figure 3. Setup and process flow of W-ELG: (a) schematic illustration (along with the definition of the coordinate system) and (b) digital picture of the experimental setup, showing the critical components of the W-ELG setup. (c) Flow chart showing the process flow of W-ELG used to create a pattern in the metal film. (d) Reaction current profile as measured at four corners of a perfectly horizontal sample (performed during the stage calibration/planarization stage). Here, the definition of horizontal orientation is defined with respect to the stylus.

Although the etching of the Cr film in both ELG and W-ELG occurs via the same principle, i.e., electric-field assisted formation of CrO_3 below the cathode tip, these two methods are fundamentally different in the sense that while ELG is a contact-based SPL technique, W-ELG is a non-contact-based SPL technique. Non-contact mode operation of W-ELG is possible due to the presence of a continuous water layer in between the cathode tip and the Cr film, whose electrolysis produces oxygen at the anode (i.e., Cr) without requiring the tip to be in contact with the film. Subsequently, oxygen reacts with Cr to form CrO_3. ELG relies on the formation of a water meniscus at the tip-substrate interface for ensuing the electrolysis and hence the chemical reaction transforming Cr into CrO_3. Hence, unlike W-ELG, ELG works in the contact mode, and that too when the relative humidity is more than a critical value. Furthermore, the need for the formation of a water meniscus in ELG precludes the usage of a blunt cathode tip.

2.2. Setup for W-ELG. Figure 3 shows the details of the setup used for selective electro-etching in the water environment and the process flowchart of W-ELG. As illustrated in Figure 3a, the W-ELG setup consists of a pointy cathode probe, which is made of tungsten (W) and can be moved over the sample in the $x-y$ (or horizontal) plane, a Z-stage that moves in the z (or vertical) direction, a water container that is placed on top of the Z-stage, and an electrical power source. A micro-positioner (manufacturer: Optimal Engineering Systems, Inc.) with a resolution of 1 μm is used for moving the tip in the $x-y$ direction, whereas the Z-stage (Manufacturer: Holmarc Opto-mechatronics Pvt. Ltd.) has a resolution of 1 μm. Both x and y motions of the micropositioner and the z motion of the Z-stage can be controlled independently using software written in Labview and appropriate software-hardware interfacing. The base of the water container is an insulating and flat Si wafer, over which 3D-printed vertical walls of the polylactic acid (PLA) polymer are glued to prevent water leakage (see Figure 3b). It should be noted that superior hardware (e.g., positioner and power source with finer resolution) can be used to obtain better control over the "writing" process and hence creating patterns with higher resolution than those reported here.

For performing W-ELG (see Figure 3c), electrical wires are connected to the two opposing edges of the sample, comprising 10−100 nm-thick Cr films deposited on the SiO_2/Si substrate. Subsequently, the sample, along with the electrical wires, is submerged into the water container. The two wires affixed to the Cr film are connected to the ground of the power source, whereas a constant negative bias is applied to the stylus, thereby making the stylus the cathode and the Cr film the anode. A constant distance between the Cr film and

https://doi.org/10.1021/acsomega.1c03858
ACS Omega 2021, 6, 25692−25701

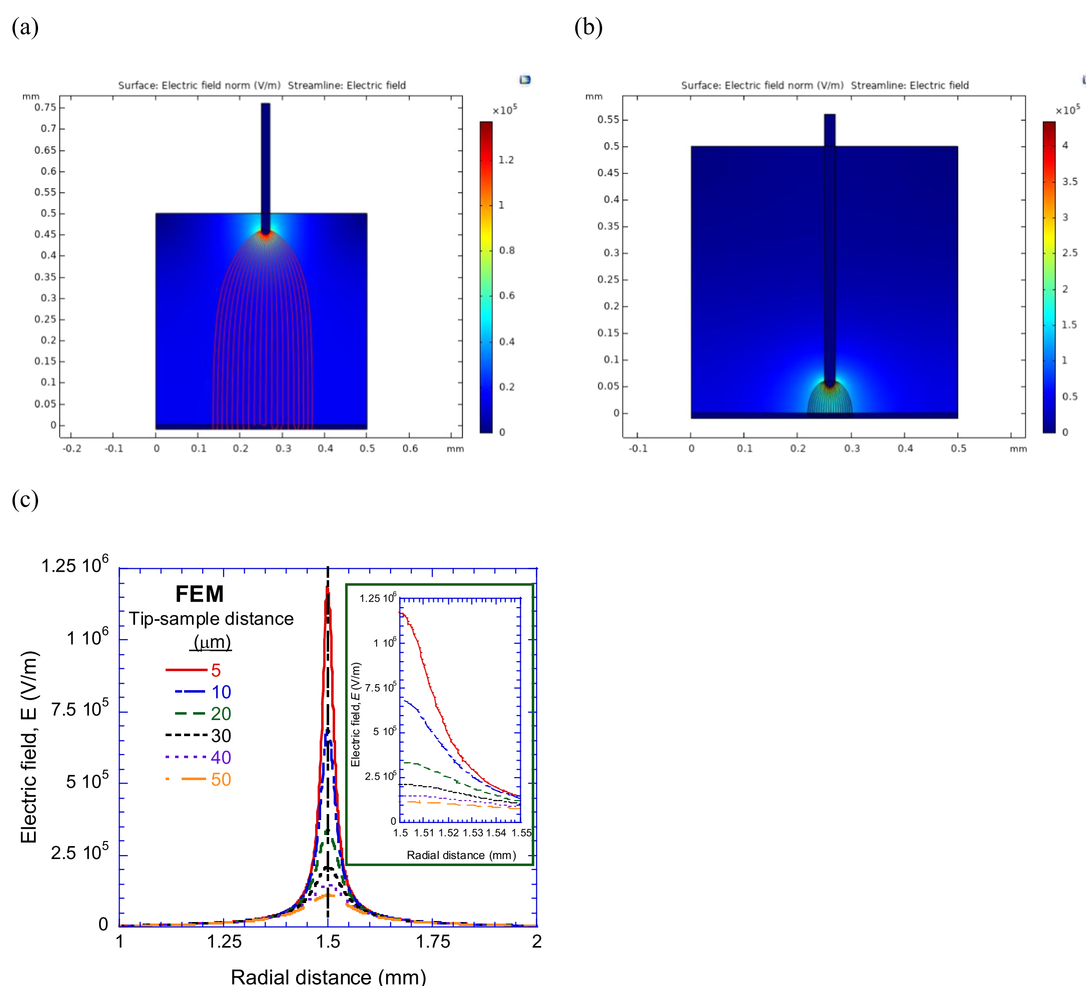

Figure 4. 2D FEM simulation results showing the effect of the tip-to-sample distance on the electric field: Electric field streamlines (depicted by red-solid curved lines) when the tip-to-sample distance is (a) 450 and (b) 50 μm, and (c) spatial variation of the electric field on the sample surface for different tip-to-sample distance. The inset on (c) shows a zoomed view near the center of the sample. The result shown in (c) is obtained from 3D simulation.

the stylus is maintained during the W-ELG process by ensuring that all locations in the sample are at a constant distance relative to the traversing stylus, thereby making the electro-etching a non-contact process. This was achieved by guaranteeing that the sample was perfectly flat relative to the stylus within its travel range.[Y] Herein, the probe tip is brought into contact with the sample at its four corners, while a small constant electrical potential is applied in between the tip and the sample, and the current is recorded at each corner. Since the contact resistance (and hence the electric current) is dependent on the contact pressure, if the current values at the four corners are the same, then the sample is assumed to be horizontal (see Figure 3d for an example current profile obtained for a sample after planarization or tip-sample calibration). Otherwise, one of the spring screws at the corners of the sample is tightened or loosened till the four current values become the same. It should be noted that the time interval over which the potential difference is applied (i.e., duration over which the tip is in contact with the sample) differed for all instances in Figure 3d; however, the quality of contact is mainly determined by the value of the reaction current. Hence, maintaining the same duration of contact at all four corners is not critical for this purpose.

Since the cathode tip is traversed along a preset locus for selectively etching the Cr film, it is important that the electric field between the cathode and the film remains constant, irrespective of the location of the tip. It was observed that when the two opposing edges of the Cr film are connected to the same bias, the electric field between the film and the stylus remains reasonably constant, even when the tip is traversed over a reasonable distance. This has been the motive for connecting electrical wires on the opposing edges of the Cr film. It should be noted that generally, the anode (or ground) in the SPM-based chemical reaction-based techniques is kept at one fixed, isolated location in the sample (or work-piece).[23,24] Since the sample behaves like a resistor, the electric current passing through the system and hence the tip-sample interaction vary depending on the distance between the tip and the location of the grounding on the sample surface. Accordingly, such a procedure for fixing the anode or ground does not guarantee patterns with uniform dimensions (see Figure S1 in the Supplemental Information for a current profile when the Cr film is grounded at an isolated location).

As the cathode tip is traversed in the non-contact mode, Cr keeps on transforming into CrO_3 via the electric field-assisted chemical reaction between Cr and water, which is spontaneously removed via its dissolution into the DI water.

https://doi.org/10.1021/acsomega.1c03858
ACS Omega 2021, 6, 25692−25701

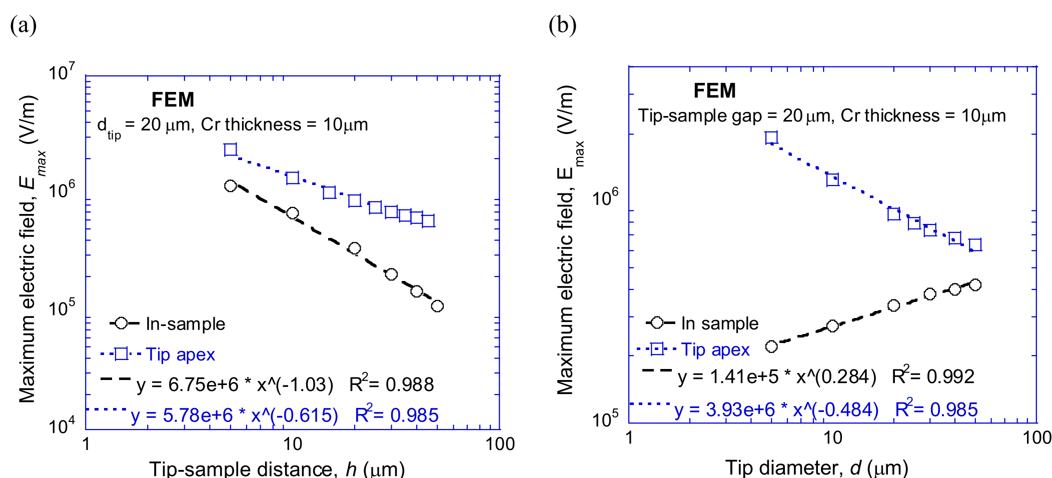

Figure 5. FEM simulation results showing the effect of process parameters: Variation of the maximum electric field at probe tip (i.e., its apex) and sample (i.e., point just below the cathode tip) as a function of the (a) tip-to-sample distance for a 20 μm diameter tip and (b) tip diameter for a tip-to-sample distance of 20 μm.

Therefore, any residue of CrO_3 is not leftover in the reaction zone and hence a clean long through-thickness trench is created in the Cr film, exposing the substrate underneath the Cr film at the selective locations. Finally, if needed, the trench pattern formed into the metal film can be transferred to the desired material by conventional thin film deposition and lift-off methods. If the substrate is transparent (e.g., glass, quartz, etc.), the created pattern can be used as a mask for photolithography.

3. RESULTS AND DISCUSSION

3.1. Process Parameter Optimization. Figure 2 suggests that the characteristics dimension of the pattern created in the Cr film would depend on the diameter of the flux "vortex" and the flux intensity. For example, if the cross section of the high-intensity flux falling onto the sample surface is smaller, then the spread of the reaction zone in the Cr film and hence the pattern dimension would also be smaller. In practice, the flux intensity and the diameter of the flux vortex near the sample would depend on the electric field at the apex of the cathode tip and the spread of the electric field on the sample, respectively. The electric field at the tip apex and the electric field profile onto the sample surface would depend on the potential difference applied between the sample, the sample-to-tip distance, and the tip diameter. Hence, before writing patterns, the effect of these process parameters on the electric field distribution is studied using COMSOL Multiphysics, a commercial finite element analysis software. Herein, a 3-dimensional model representing the tip-sample configuration in the water container (see Figure 3) is adopted for the simulation. The dimensions of the water layer and Cr film are taken to be $3 \times 3 \times 0.5$ mm^3 and $3 \times 3 \times 0.01$ mm^3, respectively. The conospherical cathode probe hangs inside the water, and its apex does not touch the Cr film. The electrical conductivities of water and Cr film are taken to be 5.5×10^{-6} and 7.9×10^6 S/m, respectively. The relative permittivities of water and Cr are taken to be 80 and 1, respectively. A physics-controlled (mixed types) 10-node tetragonal-type element of size 0.6 to 60 μm is used for discretizing the model. The "Electric Current Module" of COMSOL Multiphysics is used for the simulation.[31] In the simulations, a limit on the maximum current that can be sustained by the tip was not considered; however, it may become an important parameter to consider and optimize if the tip diameter becomes very small (e.g., a few nanometers).

A typical simulation result showing the electric field streamlines between the cathode tip and the sample is shown in Figure 4. For clarity in representation, Figures 4a,b show simulation results for a 2D model; however, all analytical results shown in this work are based on 3D simulations. As expected, the electric field streamlines spread out of the apex of the cathode tip, and their spread on the sample is more if the tip-to-sample distance is higher. Since the electric field streamlines in the W-ELG setup represent the flow of the oxygen ions generated at the cathode toward the anode sample, a larger tip-to-sample distance may lead to the chemical reaction in Cr over a larger area. However, the rate of the chemical reaction of Cr and oxygen at the anode also depends on the electric field at a location in the Cr film and hence examining the variation of the electric field in Cr is also important. Figure 4c shows the effect of the tip-to-sample distance on the electric field profile over the sample surface. In Figure 4c, the radial distance of 1.5 mm lies just below the apex of the tip. Figure 4c readily shows that the electric field on the sample surface is not uniform, and it decays non-linearly away from the center of the sample (defined as the point directly below the apex of the tip). As is evident in Figure 4c, both the maximum electric field and the span of the high-intensity electric field in the sample decrease with an increase in the tip-to-sample distance. This suggests that although the spread of the reactant would be over a larger area on Cr if the tip-to-sample distance is high, the rate of reaction may be slow. In conclusion, if a wider pattern needs to be created without increasing the tip potential, the tip-to-sample distance should be kept high, and the tip should be traversed at a slower rate.

Figure 5 shows the effect of the tip-to-sample distance and the tip diameter on the electric field at the apex of the probe tip and the maximum electric field on the surface of the Cr film. Figure 5 readily reveals that irrespective of the tip-to-sample distance and the tip diameter, the electric field at the apex of the tip is significantly more than the maximum electric field in the sample. This is attributed to the difference in the shape of these two electrodes: while the cathode is a conospherical tip, the anode is flat. This leads to the splitting

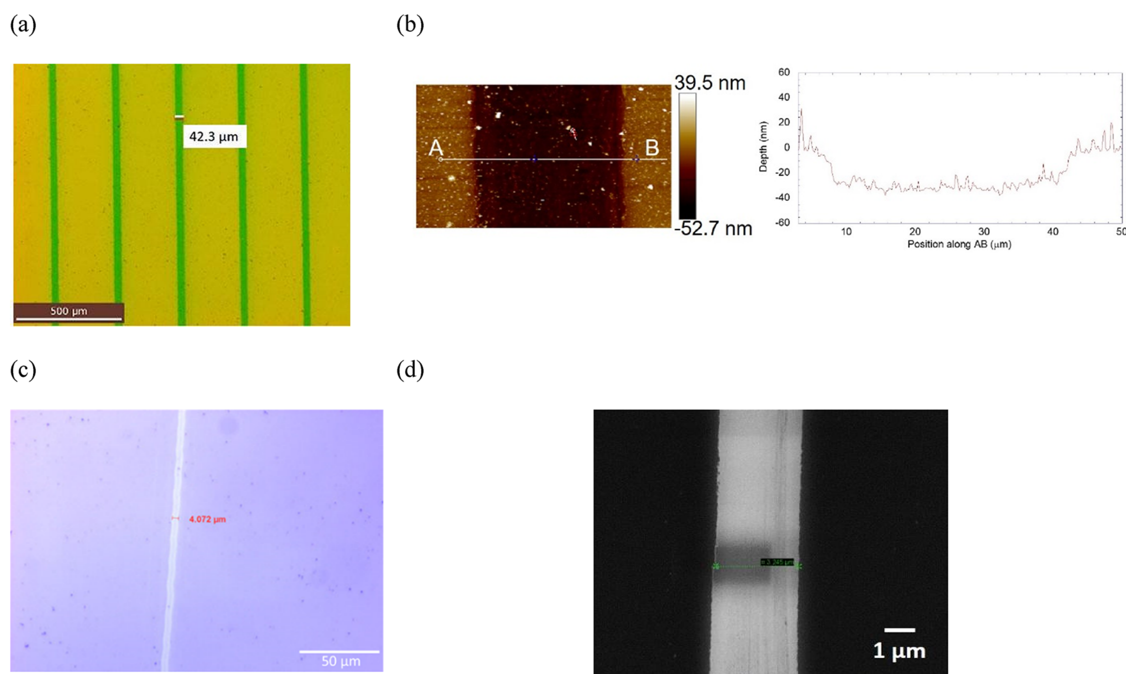

Figure 6. A few example straight-line patterns drawn in Cr film using W-ELG performed with a W-tip of 20 μm diameter (see Video S3 for a real-time video of pattern drawing in Cr using W-ELG): (a) Set of very long wide parallel patterns, having an average width of 42 μm, (b) surface topograph and the corresponding depth profile of one of the trenches shown in (a), (c) 4 μm wide pattern that is drawn by adjusting the tip-to-sample distance to $\leq$10 μm, and (d) SEM micrograph of a 3 μm wide pattern. All patterns were created using the same setup.

of water molecules preferentially at the cathode, thereby releasing a storm of the oxygen ions at the cathode that moves toward the anode for electro-etching Cr. This is evident as the flux vortex at the cathode tip (see Figure 2d and the corresponding video).

As is evident from Figure 5, the electric field at the apex of the tip increases with a decrease in the tip-to-sample distance as well as the tip diameter. Hence, an intense flux of the reactants (oxygen ions) will be produced at the cathode when a small tip is used, especially in the close proximity of the sample. On the other hand, the maximum electric field in the sample decreases with an increase in the tip-to-sample distance and a decrease in the tip diameter (see Figure S2 in the Supplemental Information for the electric field profile over the sample surface for the cathode tips of various diameters). While the implication of variation with the tip-to-sample distance on the rate of the chemical reaction is clear (i.e., a shorter tip-to-sample distance for the enhanced rate of reaction in Cr film, as it enhances both the electric field at the apex of tip and the maximum electric field in the Cr film), it appears that an optimum tip diameter needs to be established for obtaining a fast reaction rate (as tip diameter has contrasting effects on the electric field at the apex of the cathode tip and the center of Cr film). Since a combination of the high value of the electric field at the apex of the tip and the maximum electric field is required for a faster reaction rate, the variation of the product of these two electric fields as a function of the tip diameter may provide some insight into the effect of tip diameter on the reaction rate. Since, as shown in Figure 5b, the dependence of the electric field at the apex on the tip diameter (exponent ~ -0.5) is stronger than that of the maximum electric field in the sample on the tip diameter (exponent $\sim$0.3), the effect of tip diameter on the apex electric field will dominate the two. Hence, a tip with a small diameter will be effective in removing the material at a faster rate. Overall, the FEM simulation results suggest that a combination of small probe diameter and low tip-to-sample distance will be required for generating patterns of high resolution. Interestingly, this combination for a given electric potential and the tip velocity would also lead to a higher rate of electro-etching and hence the throughput will also be increased for the same combination.

3.2. Pattern Creation in Cr Using W-ELG. Figure 6 shows micrographs of a few example patterns created in a 30 nm-thick Cr film deposited on the SiO_2/Si substrate by W-ELG using a W-tip of 20 μm diameter (see Video S3 for a real-time video of pattern drawing in Cr using W-ELG). The average width of the trench is equal to 40 μm when W-ELG is performed using a tip bias of 5−10 V and a tip velocity of 300 μm/s (see Figures 6a,b). The straight-line patterns are smooth, and the residual reaction product is not observed in or at the edges of the trench and the cathode tip, unlike ELG. This unique feature of W-ELG removes the tedious task of debris-cleaning and makes the next process (such as pattern transfer) very easy. By adjusting the tip-to-sample gap to $\leq$10 μm while keeping other process parameters (such as electric potential, tip diameter, etc.) constant, patterns with characteristics dimension of $\sim$4 μm can be created (see Figure 6c), which is almost an order of magnitude smaller than that shown in Figure 6a, at a speed of 1000 μm/s, which is $\sim$3 times greater than the speed used to create the pattern shown in Figure 6a. The high-speed patterning resulted in a throughput of $\sim 1.5 \times 10^7$ μm^2/h. This reduction in the pattern width through decreasing the tip-to-sample distance while maintaining a fast velocity of the tip is consistent with the FEM simulation results (i.e., lower tip-to-sample distance reduces the spread of reactants on Cr and increases the reaction rate). Hence, besides the flexibility of ELG of changing the dimensions of the pattern using the same setup by merely varying the tip-sample potential difference and tip diameter, W-ELG has an added

flexibility of tip-to-sample distance for varying the sample dimensions. It should be noted that in W-ELG, the diameter of the reactant flux vortex is an important parameter that determines the width of the pattern, and the tip-to-sample gap, besides tip diameter, affects the flux-diameter (see Figures 4 and 5).

Figure 6d shows an SEM micrograph of a straight-line pattern of width 3 μm, which is the narrowest line drawn by W-ELG using the setup developed in this work. On the other hand, continuous and clean patterns could be created at a tip traversing speed of as high as >1500 μm/s.

In this work, tip damage was not observed during WELG patterning. Figure 7 shows a W-ELG tip (made of W) used for pattern drawing. There is no trace of tip damage even after drawing a number of patterns using this tip.

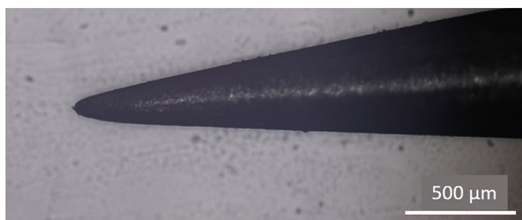

Figure 7. Optical image of a tungsten (W) tip used for pattern drawing using W-ELG. The image is taken after multiple patterns drawn by the same tip using W-ELG.

3.3. Outlook of W-ELG. Based on the throughput-resolution combination achieved by W-ELG using the semi-automatic tool developed in this work, Figure 8 is prepared,

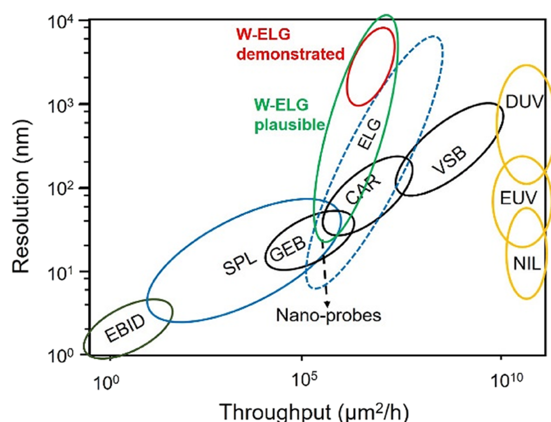

Figure 8. Comparison of W-ELG with other well-established lithography techniques using resolution-throughput criterion. The spread of all lithography techniques, except for W-ELG, was obtained from ref 23.

comparing W-ELG with other well-established lithography techniques on the throughput-resolution plot. It should be noted that both the throughput and the resolution of W-ELG can be further amplified by dedicated technological development, e.g., using high-resolution positioners, high-resolution power source, better software-hardware control system, optimized W-ELG parameters, etc. For example, a W-ELG tool for nanoscale patterning can be built using a high-end nanopositioner with a sophisticated control system, provision for utilizing an AFM tip, an automated Z-translation stage, and a detailed software-hardware user interface. It is expected that the cost of such a W-ELG tool would be not more than 3 times that of the current W-ELG tool used for micro-scale patterning, with majority of additional cost incurred in developing the nano-positioner and associated control system. This will still be significantly less than other lithography tools used for nano-scale patterning, e.g., EBL. Hence, both the demonstrated (as in this study) and the plausible (as after process optimization and hardware-software upgrades) throughput-resolution regions for W-ELG are depicted in Figure 8. W-ELG also has the added advantages of the lower cost of installation and maintenance and the flexibility over EUV and DUV. Furthermore, unlike photolithography and EBL, W-ELG is a one-step direct lithography process: It does not require a separate step of development to create patterns. The pattern is developed while writing itself due to the dissolution of the "Cr compound resist" in water. As suggested by the FEM simulation, the resolution of W-ELG can be further improved by reducing the tip diameter and working at a smaller tip-to-sample distance. It can be improved by tuning the tip traversing velocity and the tip potential also. It should be noted that a tip of 20 μm diameter was used to write 3 μm pattern shown in Figure 6c, and it is imperative that patterns of sub-micrometer, and potentially nanometer, resolutions can be obtained if the tip diameter is reduced to sub-micrometers or nanometers. Hence, W-ELG is quite promising in being developed as a versatile lithography technique that is economical and flexible (or batch customizable) and suitable for producing high-resolution patterns at high throughput. Due to the availability of several independent process parameters, such as sample-tip distance, applied tip potential, tip velocity, tip diameter, etc., that affect the resolution and the throughput, it can be speculated that Tennant's law will be less severe for W-ELG. Hence, the W-ELG appears a bit more vertical on the resolution-throughput plot.

There are various fundamental aspects that make W-ELG a unique problem solver. The chemical compound formed on the surface of Cr is CrO_3, which readily dissolves in water during the pattern drawing.[30] Hence, unlike other such chemical reaction-based SPL processes, the reaction product neither stays in the reaction zone nor sticks to the tip during W-ELG. Therefore, W-ELG does not suffer from the issue of debris accumulation and produces clean patterns. Furthermore, the pattern in the Cr film is drawn only due to the chemical reaction induced by the electric field, while the tip traverses in non-contact mode. This precludes any physical damage to the tip and the substrate, including scratching and plowing of the thin metal film. Therefore, the obtained patterns are free of any debris, and the life of the "writing" tip is very high (see Figure 7). This (i.e., alleviation of the tip damage) also guarantees the high repeatability of patterns created in two batches. Furthermore, since the process requires only DI water as the medium, it is eco-friendly. DI water is also non-corrosive and available in more abundance than any other liquid medium. Finally the chemistry at the cathode is immune to local fluctuations in the ambiance conditions (i.e., temperature, humidity, etc.).

The edge of the line pattern is round (see Figures 2b and 6c), which is in contrast to the relatively sharp edge of the trenches created using the standard electrolithography process, including SPL. The rounded profile of the edge in the W-ELG process can be attributed to the decrease in the kinetics of the chemical reaction, and hence the rate of the material removal, away from the center of the sample (i.e., the point just below

the tip) (see Figure 4c). Since the material removal rate in W-ELG is significantly faster than the standard electrolithography process, a minor difference in the electric field or flux density at various locations may show a noticeable difference in the material removal rate. In practice, the rounding of the edges of the trenches in the W-ELG process would be beneficial during pattern transfer during wet or dry etching of the layer below the Cr film. The etchant must hit the layer to be etched away, which is much easier for patterns with a wider opening on the top surface.

It should be noted that the developed W-ELG cannot be treated as an extension to the SPL techniques based on STM and AFM, as W-ELG uses a considerable volume of water in between the tip and the sample and also the tip-to-sample distance can be as high as several tens of micrometers; standard STM and AFM are not designed to work under these conditions. Due to the need for maintaining a significant distance between the tip and the sample, which can vary over several orders of magnitude (e.g., a few tens of nanometers for an ultrahigh resolution to a few tens of micrometers for writing wide patterns), developing a dedicated and robust control system to be fitted into W-ELG equipment remains an open challenge. However, it can be met through focused technology development.

4. CONCLUSIONS

The invention of a new tip-based lithography technique, named water-electrolithography (W-ELG), is described in this work. W-ELG provides a non-contact mode for pattern drawing via electro-etching of a Cr film deposited on a substrate and submerged into water, at a throughput of up to $\sim 10^7$ μm^2/h with a resolution of 4 μm. Since it "writes" in the non-contact mode and the reaction product readily dissolves away into the water, W-ELG resolves the existing SPL-related issues of tip damage, sample damage, debris accumulation at the patterned sites, and limited repeatability of patterns.

Pattern resolution is primarily dependent on the diameter of the reactant flux falling onto the sample, which is a function of the tip diameter, the tip-to-sample distance, and the electric potential applied between the tip and the sample. For a given tip potential and tip velocity, a combination of small tip-to-sample distance and small tip diameter is favorable for creating high-resolution patterns at reasonably high throughput.

The potential of low-cost, eco-friendly, and sustainable lithography tool development and easy handling of W-ELG make it quite promising. W-ELG is feasible for scaling and has the potential of producing the devices requiring high-resolution patterning at a lower cost and higher throughput.

■ ASSOCIATED CONTENT

Supporting Information

The Supporting Information is available free of charge at https://pubs.acs.org/doi/10.1021/acsomega.1c03858.

Supporting Information Video 1: Video showing electro-etching of a Cr film with a water droplet placed between the cathode and the Cr film (MP4)

Supporting Information Video 2: Video showing formation of a vortex like feature during electro-etching of the Cr film submerged into water (MP4)

Supporting Information Video 3: Video showing patterning of multiple lines in the Cr film using W-ELG (MP4)

Plots showing the effects of grounding of the sample at an isolated location on the reaction current and the tip diameter on the profile of the electric field on the surface of the sample (PDF)

■ AUTHOR INFORMATION

Corresponding Author

Praveen Kumar − *Department of Materials Engineering, Indian Institute of Science, Bangalore 560012, India;* orcid.org/0000-0002-8890-9969; Email: praveenk@iisc.ac.in

Authors

Sumit Kumar − *Center for Nano-Science and Engineering, Indian Institute of Science, Bangalore 560012, India*

Ebinesh Abraham − *Center for Nano-Science and Engineering, Indian Institute of Science, Bangalore 560012, India*

Rudra Pratap − *Center for Nano-Science and Engineering, Indian Institute of Science, Bangalore 560012, India*

Complete contact information is available at: https://pubs.acs.org/10.1021/acsomega.1c03858

Notes

The authors declare no competing financial interest.

■ ACKNOWLEDGMENTS

The authors would like to acknowledge the financial support provided by DSTO 1526 (Technology System Development Program of Department of Science and Technology, India) and DSTO 1759 (Indo-Russia Joint Research Project of Program of Department of Science and Technology, India). The authors thank Dr. Mrutyunjay Swamy and Mr. Raman Maurya of the Indian Institute of Science, Bangalore, for useful discussions.

■ DEDICATION

This paper is dedicated to Mr. Randhir Kumar (1985−2021), our colleague at the Indian Institute of Science, Bangalore. He immensely helped us conduct this work, but unfortunately departed to heaven just before the finalization of this manuscript.

■ ADDITIONAL NOTES

[$]Batch customizability here is defined as the ability of the lithography technique to create two consecutive patterns or batches of patterns different from each other using the same hardware, with minimal changes in the process parameters. It also includes creating patterns with widely different feature sizes.

[£]ELG is a recently invented lithography technique that relies on the etching of Cr film at the cathode tip through an electro-chemical process. Herein, two pointy electrodes are placed on the Cr film deposited on a non-conducting substrate (such as SiO_2/Si, glass, etc.) and a potential difference is applied between the electrodes. Upon application of an electric potential, the Cr film below the cathode reacts with water vapor present in the ambient to form CrO_3.[30] The reaction zone moves away from the cathode in a radially symmetric fashion. This process, therefore, creates a through-thickness trench in the Cr film near the cathode. If the cathode is traversed along a set locus while keeping the anode stationary,

a continuous trench gets created in the Cr film, thereby creating a pattern.[24]

€Limited parallelization of EBL through splitting of the primary electron beam and controlling the split beams independently has been demonstrated.[32] However, such a provision is yet to widely adapted and available in the standard EBL setups.

¥Placing a polished Si wafer as the base of the water container is quite critical in maintaining a constant distance between the stylus and the sample.

■ REFERENCES

(1) Stevenson, J. T. M.; Gundlach, A. M. The Application of Photolithography to the Fabrication of Microcircuits. *J. Phys. E.* **1986**, *19*, 654−667.

(2) Luo, C.; Xu, C.; Lv, L.; Li, H.; Huang, X.; Liu, W. Review of Recent Advances in Inorganic Photoresists. *RSC Adv.* **2020**, *10*, 8385−8395.

(3) Chen, Y. Nanofabrication by Electron Beam Lithography and Its Applications: A Review. *Microelectron. Eng.* **2015**, *135*, 57−72.

(4) Xia, Y. Whitesides. G. M: Soft Lithography. *Angew. Chem., Int. Ed. Engl.* **1998**, *37*, 550−575.

(5) Wu, B.; Kumar, A. Extreme Ultraviolet Lithography: A Review. *J. Vac. Sci. Technol., B: Microelectron. Nanometer Struct. −Process,. Meas., Phenom.* **2007**, *25*, 1743−1761.

(6) Garcia, R.; Knoll, A. W.; Riedo, E. Advanced Scanning Probe Lithography. *Nat. Nanotechnol.* **2014**, *9*, 577−587.

(7) Ryu, Y. K.; Garcia, R. Advanced Oxidation Scanning Probe Lithography. *Nanotechnology* **2017**, *28*, 142003−142020.

(8) Pimpin, A.; Srituravanich, W. Reviews on Micro- and Nanolithography Techniques and Their Applications. *Eng. J.* **2012**, *16*, 37−56.

(9) Manfrinato, V. R.; Zhang, L.; Su, D.; Duan, H.; Hobbs, R. G.; Stach, E. A.; Berggren, K. K. Resolution Limits of Electron-Beam Lithography toward the Atomic Scale. *Nano Lett.* **2013**, *13*, 1555−1558.

(10) Wu, B.; Neureuther, A. R. Energy Deposition and Transfer in Electron-Beam Lithography. *J. Vac. Sci. Technol. B: Microelectron. Nanometer Struct.—Process. Meas., Phenom.* **2001**, *19*, 2508−2511.

(11) Bolorizadeh, M.; Joy, D. C. Effects of Fast Secondary Electrons to Low-Voltage Electron Beam Lithography. *J. Micro/Nanolithogr., MEMS, MOEMS* **2007**, *6*, 023004−023010.

(12) Tennant, D. M. Limits of Conventional Lithography. *Nanotechnology* **1999**, 161−205.

(13) Seisyan, R. P. Nanolithography in Microelectronics: A Review. *Tech. Phys.* **2011**, *56*, 1061−1073.

(14) Taguchi, A.; Nakayama, A.; Oketani, R.; Kawata, S.; Fujita, K. Multiphoton-Excited Deep-Ultraviolet Photolithography for 3D Nanofabrication Atsushi. *ACS Appl. Nano Mater.* **2020**, *3*, 11434−11441.

(15) Ausschnitt, C. P.; Thomas, A. C.; Wiltshire, T. J. Advanced DUV Photolithography in a Pilot Line Environment. *IBM J. Res. Dev.* **1997**, *41*, 21−37.

(16) Bratton, D.; Yang, D.; Dai, J.; Ober, C. K. Recent Progress in High Resolution Lithography. *Polym. Adv. Technol.* **2006**, *17*, 94−103.

(17) Soufli, R.; Baker, S. L.; Gullikson, E. M.; McCarville, T.; Robinson, J. C.; Martínez-Galarce, D.; Fernández-Perea, M.; Pivovaroff, M. J. Review of Substrate Materials, Surface Metrologies and Polishing Techniques for Current and Future-Generation EUV/x-Ray Optics. *Adv. Metrol. X-Ray EUV Opt. IV* **2012**, *8501*, 850102−850111.

(18) Kondo, S.; Heike, S.; Lutwyche, M.; Wada, Y. Surface Modification Mechanism of Materials with Scanning Tunneling Microscope. *J. Appl. Phys.* **1995**, *78*, 155−160.

(19) Lenk, C.; Hofmann, M.; Lenk, S.; Kaestner, M.; Ivanov, T.; Krivoshapkina, Y.; Nechepurenko, D.; Volland, B.; Holz, M.; Ahmad, A.; Reum, A.; Wang, C.; Jones, M.; Durrani, Z.; Rangelow, I. W. Nanofabrication by Field-Emission Scanning Probe Lithography and Cryogenic Plasma Etching. *Microelectron. Eng.* **2018**, *192*, 77−82.

(20) Kalinin, S. V.; Gruverman, A. *Scanning Probe Microscopy Electrical and Electromechanical Phenomena at the Nanoscale*; Springer Science & Business Media, 2003.

(21) Song, H. J. 25 Nm Chromium Oxide Lines By Scanning Tunneling Lithography in Air. *J. Vac. Sci. Technol. B: Microelectron. Nanometer Struct.–Process., Meas., Phenom.* **1994**, *12*, 3720.

(22) Xie, W.; Dai, X.; Xu, L. S.; Allee, D. A.; Spector, J. Fabrication of Cr Nanostructures with the Scanning Tunnelling Microscope. *Nanotechnology* **1997**, *8*, 88−93.

(23) Talukder, S.; Kumar, P.; Pratap, R. Electrolithography- A New and Versatile Process for Nano Patterning. *Sci. Rep.* **2016**, *5*, 1−11.

(24) Kumar, S.; Abraham, E.; Talukder, S.; Kumar, P.; Pratap, R. Micro Electrolithography System Development. In 2018 *4th IEEE International Conference on Emerging Electronics, ICEE 2018*; IEEE, *2018*; pp. 1−4.

(25) Salaita, K.; Wang, Y.; Fragala, J.; Vega, R. A.; Liu, C.; Mirkin, C. A. Massively Parallel Dip−Pen Nanolithography with 55 000-Pen Two-Dimensional Arrays. *Angew. Chem.* **2006**, *118*, 7378−7381.

(26) Zhang, M.; Bullen, D.; Chung, S. W.; Hong, S.; Ryu, K. S.; Fan, Z.; Mirkin, C. A.; Liu, C. A MEMS Nanoplotter with High-Density Parallel Dip-Pen Nanolithography Probe Arrays. *Nanotechnology* **2002**, *13*, 212−217.

(27) Wang, D.; Tsau, L.; Wang, K. L.; Chow, P. Nanofabrication of Thin Chromium Film Deposited on Si(100) Surfaces by Tip Induced Anodization in Atomic Force Microscopy. *Appl. Phys. Lett.* **1995**, *67*, 1295.

(28) Rolandi, M.; Quate, C. F.; Dai, H. A New Scanning Probe Lithography Scheme with a Novel Metal Resist. *Adv. Mater.* **2002**, *14*, 191−194.

(29) Huh, C.; Park, S.-J. Atomic Force Microscope Tip-Induced Anodization of Titanium Film for Nanofabrication of Oxide Patterns. *J. Vac. Sci. Technol. B: Microelectron. Nanometer Struct.–Process., Meas., Phenom.* **2000**, *18*, 55.

(30) Kumar, S.; Suresh, H.; Sethuraman, V. A.; Kumar, P.; Pratap, R. Electric Field Induced Patterning in Cr Film under Ambient Conditions : A Chemical Reaction Based Perspective. *SN Appl. Sci.* **2020**, *2*, 1−9.

(31) Benziada, M. A.; Boubakeur, A.; Mekhaldi, A. Numerical Simulation of the Barrier Effect on the Electric Field Distribution in Point-Plane Air Gaps Using COMSOL Multiphysics. In *The 5th International Conference on Electrical Engineering − Boumerdes (ICEE-B)*; 2017; pp. 1−6.

(32) Chang, T. H. P.; Mankos, M.; Lee, K. Y.; Muray, L. P. Multiple Electron-Beam Lithography. *Microelectron. Eng.* **2001**, *57-58*, 117−135.

https://doi.org/10.1021/acsomega.1c03858
ACS Omega 2021, 6, 25692−25701